Studies on structural, optical, magnetic, and resistive switching properties of doped BiFe$_{1-x}$Cr$_x$O$_3$ thin films

Y. Sharma, R. Martinez, R. Agarwal, D. Barrionuevo, R. K. Katiyar, A. Kumar, and R. S. Katiyar

Studies on structural, optical, magnetic, and resistive switching properties of doped BiFe$_{1-x}$Cr$_x$O$_3$ thin films

Y. Sharma,[1] R. Martinez,[1,2] R. Agarwal,[1] D. Barrionuevo,[1] R. K. Katiyar,[1] A. Kumar,[3] and R. S. Katiyar[1]

[1]*Department of Physics and Institute for Functional Nanomaterials, University of Puerto Rico, San Juan, Puerto Rico 00936-8377, USA*
[2]*Department of Mathematics and Physics, University of Puerto Rico, Cayey, Puerto Rico 00736, USA*
[3]*CSIR-National Physical Laboratory, Dr. K.S. Krishnan Marg, Delhi, India*

We report the effect of multivalent Cr-ion doping on the structural, optical, magnetic, and resistive switching properties of BiFe$_{1-x}$Cr$_x$O$_3$ (BFCO) thin films (where, $0 \leq x \leq 0.15$). BFCO thin films were deposited on Pt/TiO$_2$/SiO$_2$/Si (100) substrate using pulsed laser deposition technique. X-ray diffraction and micro-Raman analysis revealed the presence of a secondary phase in BFCO thin films, above 5% Cr doping concentrations. Enhanced magnetization was observed in BFCO films owing to ferromagnetic superexchange interaction between Fe and Cr-ions. X-ray photoelectron spectroscopy measurements revealed the multivalent states of Cr and Fe-ions, where suppression of oxygen vacancies due to Cr-ion doping in BFCO films was discussed based on the defect chemistry viewpoint. Moreover, current conduction and resistive switching properties were studied and the dominant switching mechanism was explained in the light of oxygen vacancies assisted filamentary conduction model. *Published by AIP Publishing*. [http://dx.doi.org/10.1063/1.4967993]

I. INTRODUCTION

The multifunctional oxide BiFeO$_3$ (BFO), which exhibits simultaneous ferroelectric, (anti) ferromagnetic, piezoelectric, ferroelastic, and flexoelectric order parameters have attracted great research attention due to potential applications towards new generation multiple states logic devices including spintronics and nonvolatile multiple-state memories.[1–6] Among other ABO$_3$-type perovskite oxides, BFO has stood out as a single phase oxide with interesting room temperature multiferroic and magnetoelectric properties.[1,4,7] Epitaxial and polycrystalline BFO thin films show significantly improved multiferroic properties, ferroelectric photovoltaics, and switchable photo-diode effect, which enable their use towards advanced optoelectronic applications as well. Nevertheless, the severe leakage current in BFO thin film, mainly due to the oxygen vacancies, created during the film growth process, greatly destroy its ferroelectric property.[8–17] From defect chemistry viewpoint, neutralization/ionization of oxygen vacancies may induce mixed valance states of Fe^{3+} and Fe^{2+} which in turn leads tunability of leakage current in BFO films.[18] Numerous attempts have been made to suppress the leakage current in BFO films, including site-engineering using substitution/doping of some elements at the Bi and/or Fe-sites.[10–12] Appropriate doping at Fe-site not only improves electrical and magnetic properties, but also gives the additional functionality as resistive switching (RS) effect in BFO thin films due to doping driven competition between energetically insulating and conducting ground states.[18,19] Variety of aliovalent transition metals have been doped at Fe-site, such as Ti, Nb, Hf, Ta, Mn, and so on, which are found to be advantageous towards improving magnetic and ferroelectric properties of doped-BFO thin films by means of complex exchange interactions between neighboring transition metal ions and

elimination of charge defects, respectively.[10–12,18,20] However, there are few studies available in the literature related to the effect of multivalent transition metal ion doping on physical properties and charge transport in BFO thin films.[18,21]

In this paper, we report the effect of Cr-doping on lattice, spin ordering, and electrical transport properties of BiFe$_{1-x}$Cr$_x$O$_3$ (BFCO) (x = 0, 0.05, 0.1, and 0.15) thin films grown by pulsed laser deposition. Structural, electrical, and magnetic properties of BiFe$_{1-x}$Cr$_x$O$_3$ (BFCO) thin films were studied with different doping concentrations of Cr-ion. The current-voltage (I-V) characteristics revealed resistive switching in these films, which was found to be highly dependent on Cr-ion doping concentration. The dominant mechanism responsible for switching phenomenon was also explained.

II. EXPERIMENTAL

BFCO thin films by varying Cr-doping concentration (0, 5, 10, and 15 at. %) were deposited on commercially available Pt/TiO$_2$/SiO$_2$/Si (100) substrate using pulsed laser deposition technique. A KrF pulsed excimer laser ($\lambda = 248$ nm) operating at a fluence of ~ 1.8 J/cm^2 and repetition rate of 5 Hz was used for ablation of single phase ceramic targets of BFCO prepared by solid state reaction method. The BFCO films of expected thickness ~ 300 nm were deposited at the fixed temperature of 720 °C and an oxygen partial pressure of ~ 200 mTorr. After deposition, BFCO films were annealed at 750 °C for 20 min in excess oxygen pressure of 400 mTorr in order to suppress the oxygen vacancy and/or enhance the crystal structure quality. To fabricate metal-insulator-metal (MIM) capacitor structure, Pt top electrodes of thickness ~ 80 nm and the diameter of ~ 200 μm were deposited at room temperature by dc-magnetron sputtering through a square metal shadow mask. The structural properties of the

films were investigated by recording x-ray diffraction pattern of the films using Rigaku Ultima *III*- x-ray diffractometer, and room temperature Raman spectra using a Jobin-Yvon T64000 triple spectrometer with grating (1800 grooves mm^{-1}), and a diode pumped solid state laser ($\lambda = 532$ nm) was used as an excitation source. Chemical compositions of as-deposited BFCO thin films were analysed by X-ray photo-electron spectroscopy (XPS). Magnetic hysteresis (M vs. H) loops of the BFCO film were recorded with a vibrating sample magnetometer (VSM, Lakeshore 7400) at room temperature. The resistance switching characteristics and conduction mechanisms of the Pt/BFCO/Pt device were studied through current-voltage (I-V) measurements in top-bottom configuration using a Keithley-2401 source-measure unit.

III. RESULTS AND DISCUSSION

A. Structural and optical properties

Figure 1(a) shows the x-ray diffraction (XRD) patterns of pure and Cr-doped BFO thin films. Hereafter, throughout the paper, pure and Cr-doped BFO samples are termed as BFO (pure), BFCO5 (5% Cr), BFCO10 (10% Cr), and BFCO15 (15% Cr), respectively. Polycrystalline rhombohedral distorted perovskite structures of pure BFO and BFCO5
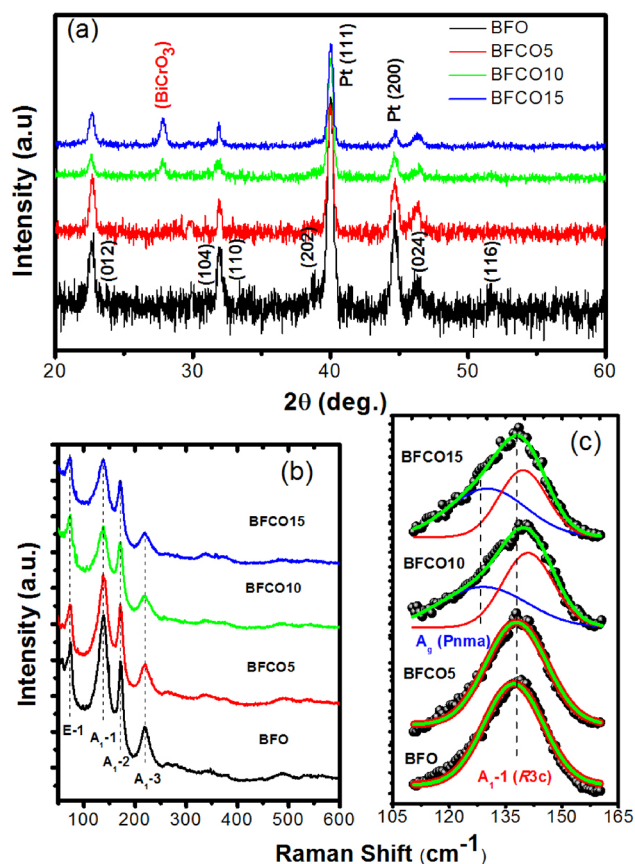

FIG. 1. (a) X-ray diffraction patterns and (b) room temperature Raman spectra of the BFO, BFCO5, BFCO10, and BFCO15 thin films, respectively, on Pt/TiO$_2$/SiO$_2$/Si (100) substrate. (c) Raman spectra in selected spectral range fitted with the sum of Lorentzian line shape. Red and blue lines show individual Lorentzian line shapes corresponding to A$_1$-1 mode of BFO (R3c) at $\sim$140 cm^{-1} and A$_g$ mode of BCO phase (Pnma) at $\sim$129 cm^{-1}, while green line is the composite fit profile.

films that appear to be single phase, are confirmed from XRD patterns. However, an additional peak around $2\theta = 28°$ was observed in XRD patterns of BFCO10 and BFC15 thin films, which could be attributed to the BiCrO$_3$ (BCO), Bi$_7$CrO$_{12.5}$ (JCPDS No. 42-0527), or Bi$_{12}$(Bi$_{0.5}$Fe$_{0.5}$)O$_{19.5}$ (JCPDS No. 80-0821) phases. It would be hard to distinguish among these phases; however, BCO and Bi$_7$CrO$_{12.5}$ may be the possible candidates, which can normally form at higher doping concentrations and moderate film growth conditions, respectively.[22] Intensity corresponding to peak near 28° Bragg's angle increases with increase in Cr-doping concentration from 10% to 15%, which indicate that high concentration of Cr-doping (above 5 at. %) leads to developing a secondary phase in BFO matrix.

To further confirm the existence of secondary BCO phase in BFCO10 and BFCO15 thin films, Raman spectroscopic analysis were carried out. Figure 1(b) shows the room temperature Raman spectra of BFO, BFCO5, BFCO10, and BFCO15, respectively. Raman spectra of BFO and BFCO5 films belonging to rhombohedral (R3c) structure, show sharp peaks corresponding to A$_1$ and E fundamental Raman modes in the spectral window of 40–600 cm^{-1}.[23] One can observe that the peak corresponding to A$_1$-1 mode at $\sim$140 cm^{-1} getting abnormal broadening as we increase Cr-concentration, and in BFCO10 and BFCO15 thin film samples, this peak can only be fitted by deconvoluting into two peaks, as shown in the inset of Fig. 1(c). Therefore, a shoulder peak at $\sim$129 cm^{-1} near to A$_1$-1 mode of BFO can be indexed as A$_g$ mode of BCO phase with orthorhombic symmetry (space group: Pnma).[24,25] Thus, the Raman spectroscopic finding of the BCO secondary phase in BFCO10 and BFCO15 thin films supports the XRD results. For the optical band gap measurement of BFO and BFCO thin films, UV-Visible transmittance spectrum was recorded in a wide wavelength range of 190–1100 nm, as shown in Fig. 2(a). The optical transmittance shows that BFO and BFCO thin films are quite transparent (between 70% and 90%) in the visible and near IR spectral region indicating low optical losses caused by absorption and scattering, as shown in Fig. 2(a). The direct band gap calculations of the BFCO films are done by a linear extrapolation of $(\alpha h\nu)^2$ versus $h\nu$ plot (where α is the absorption coefficient and ($h\nu$) is incident photon energy). The resulting plot has a distinct linear regime which denotes the onset of absorption. Thus, extrapolating this linear region to the $h\nu$ abscissa yields the energy of the optical band gap of the films, as shown in the inset of Fig. 2(b). The band gap (E$_g$) of the BFCO10 (2.68 eV) and BFCO15 (2.71 eV) films was found to be substantially higher as compared to BFO (2.60 eV) and BFCO5 (2.63 eV) films, which can further support the presence of secondary BCO phase, as the direct optical band gap of BCO ($\sim$2.95 eV) is higher compared to pure BFO ($\sim$2.62 eV).[9,10] Optical results further strengthen our observation that increasing Cr concentration beyond a certain limit stabilized a secondary BCO phase in BFO matrix.

B. Magnetization behavior

Figure 3 shows out of plane magnetic hysteresis (M-H) loops obtained for the BFO and BFCO films at room
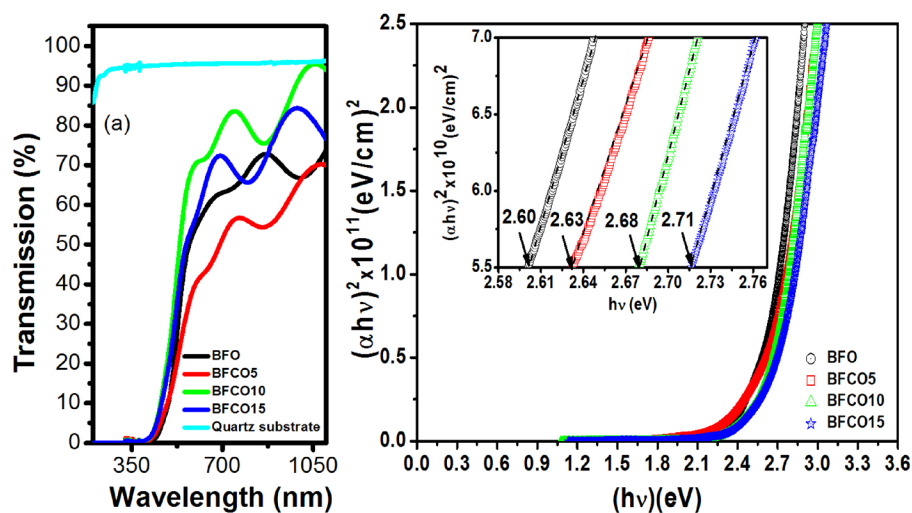
FIG. 2. (a) Optical transmittance of the BFO, BFCO5, BFCO10, and BFCO15 thin films deposited on quartz substrate. (b) The plot of $(\alpha h\nu)^2$ versus phonon energy ($h\nu$), where inset shows the linear extrapolation of the plot to zero, determining the variation of band gap (E_g) with Cr-doping concentration.

temperature. The value of saturation magnetization (M_S) in BFO and BFCO5 films is found to be nearly same ~ 26 and $28 \, emu/cm^3$, respectively, which is high enough as compared to previous reports on BFO and BFCO thin films around same doping concentrations.[26,27] It has been observed that Cr dopant can distort the long-range cycloidal spin arrangement of BFO and enhance the magnetization via valence effect. Such high magnetization in BFO films can also be attributed to the presence of Fe^{2+} ions[26,28] and/or to strain induced increase in spin canting angle. We noted that magnetization further increases in BFCO10 sample and the value of M_S was found to be nearly two times ($\sim 60 \, emu/cm^3$) as compared to BFO and BFCO5 samples. The possible reason for enhanced magnetization in BFCO10 sample could be the ferromagnetic interaction between e_g electrons of Fe^{3+} and the t_{2g} electrons of the Cr^{3+} ions.[29] Surprisingly, we observed that the value of M_S is decreased in case of BFCO15 sample and found to be $\sim 39 \, emu/cm^3$. This unusual magnetic behavior in BFCO15 sample with highest Cr-concentration can be explained in terms of the structural instability as confirmed from XRD and Raman spectroscopic studies. The increased phase mixture of BFO and BCO phases especially in BFCO15 film having highest Cr-doping percentage, can potentially change the

metal-oxygen bond angles, where the deviation in Fe–O–Cr bond angle from perfect $180°$ makes Cr t_{2g} and Fe e_g interaction no longer ferromagnetic, resulting in a decrease in M_S for BFCO15 film.[29,30] Furthermore, the presence of multivalence states of transition metal ions, which we will be discussing in Sec. III C, can also explain the change in magnetization in our BFCO thin films, where the magnetic moment in BFCO15 film can be decreased through the disruption of ferromagnetic superexchange interactions along the Fe^{2+}–O–Cr^{4+}–O–Fe^{3+} bond.[29]

C. Resistive memory switching

To explore the charge transport and conduction behavior, current-voltage (I-V) measurements were carried out on metal–insulator–metal (MIM) capacitor structure of BFO and BFCO thin films. A schematic diagram of Pt/BFO/Pt or Pt/BFCO/Pt device is represented in Fig. 4(a). I-V characteristics of BFO, BFCO5, BFCO10, and BFCO15 based devices were shown in semi-logarithmic plot in Fig. 4(b). Interestingly, we observed unipolar resistance switching (URS) only in BFO and BFCO5 films under DC bias sweeping voltage of 0–10 V, whereas BFCO10 and BFCO15 films do not show any sudden change in resistance values. It can be seen that leakage current is significantly reduced with increased Cr-concentration, where the leakage current value (at 2 V) in BFCO15 film was found to be two orders of magnitude less than the pure BFO film. In pristine state, like BFCO10 and BFCO15 films, BFO and BFCO5 films were also found to be insulating with resistance value of $\sim 12 \, M\Omega$ (read at 0.1 V). Whereas, the so-called "electroforming process" drives the BFO and BFCO5 based devices into low resistance state (LRS) with a resistance ~ 60 and $110 \, \Omega$ (read at 0.2 V), respectively, and the current flowing through the devices was found to be abruptly increased at around 4.7 and 5.2 V, respectively, as shown in Fig. 4(b). A current compliance (I_{CC}) = 1 mA was kept fixed during electroforming to prevent the devices from permanent dielectric breakdown due to high current flow in LRS.[31] Further, in case of BFO and BFCO5 devices, as the voltage was again swept from 0 to 2 V, a rapid decrease in current was observed at a voltage of ~ 1.2 and 1.6 V, respectively, representing that both of the
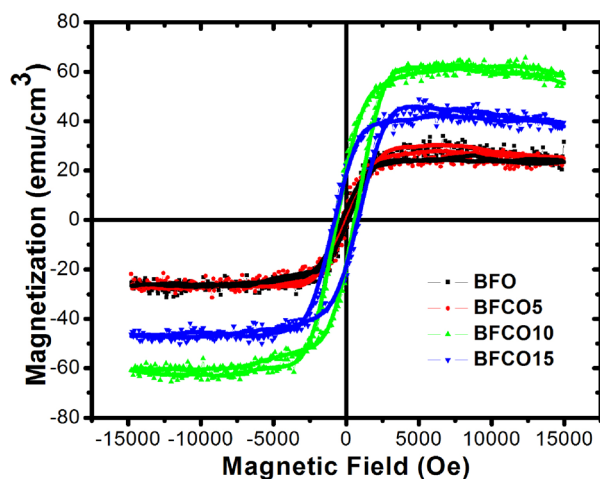

FIG. 3. Magnetic hysteresis (M-H) loops of the BFO, BFCO5, BFCO10, and BFCO15 thin films at room temperature.
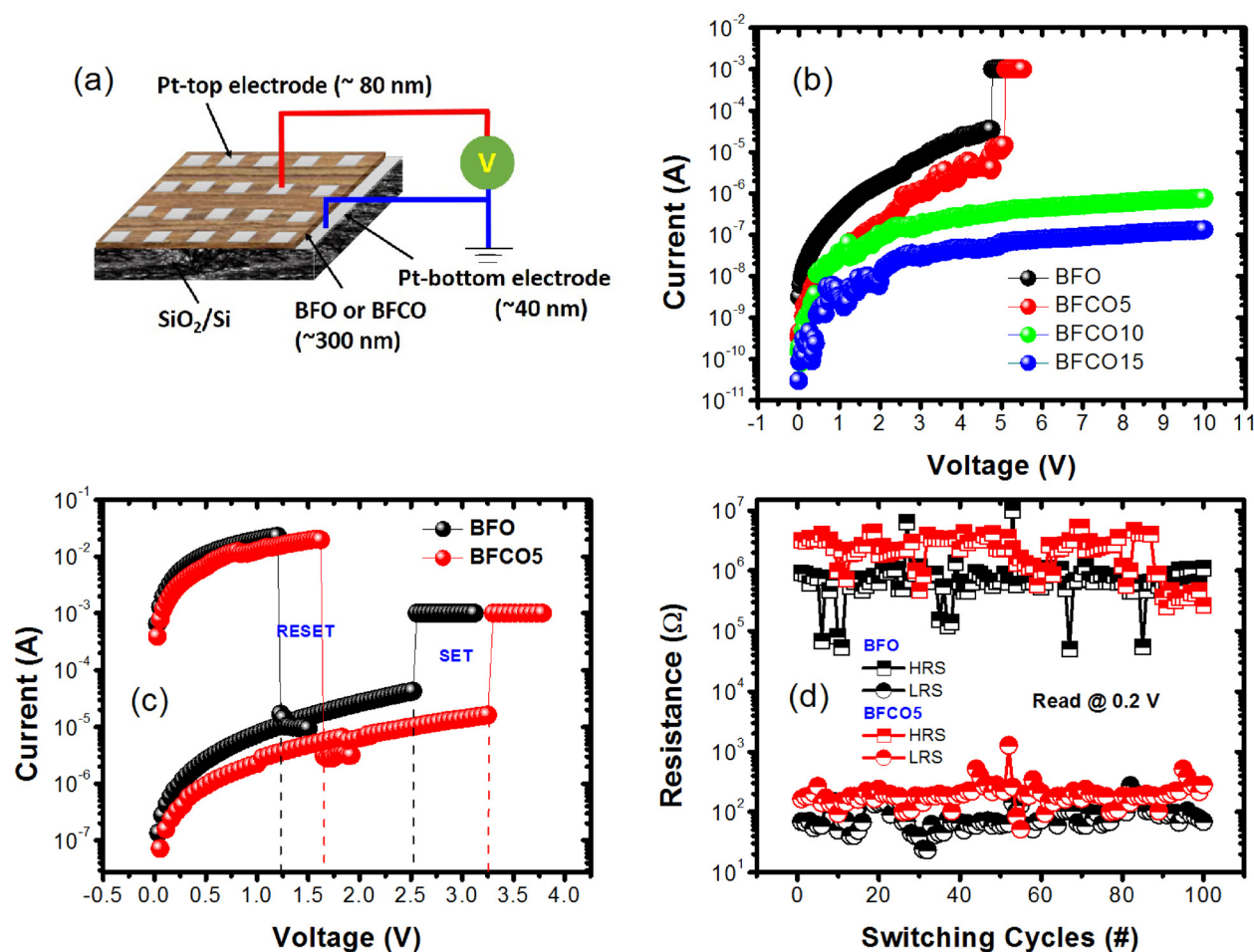
FIG. 4. (a) Schematic of Pt/BFO/Pt or Pt/BFCO/Pt device for resistive switching measurements. (b) I-V characteristics of the BFO, BFCO5, BFCO10, and BFCO15 thin films. (c) Typical I-V characteristic of the Pt/BFO/Pt and Pt/BFCO5/Pt resistive switching devices showing unipolar resistive switching behavior. (d) The endurance of Pt/BFO/Pt and Pt/BFCO5/Pt devices over 100 consecutive cycles.

devices are switched to high resistance state (HRS), as shown in Fig. 4(c). In HRS, as the voltage was swept again from 0 to 4 V, a sudden increase in current was observed at ~2.5 and 3.3 V, respectively, and both of the devices are switched back into LRS. To confirm the repeatability of switching of resistance states, we investigated the endurance characteristics of the devices. The endurance characteristics of both the devices under a fixed $I_{CC} = 1$ mA has been performed up to 100 consecutive switching cycles, as shown in Fig. 4(d). The well separated resistance values of HRS and LRS with resistance ratio of ~10^3 were read at 0.2 V. Thus, a repeatable non-volatile unipolar switching of the resistance is demonstrated in Pt/BFO/Pt and Pt/BFCO5/Pt devices.

Moreover, a detailed understanding of the resistive switching mechanism is very necessary in controlling resistive random access memory (RRAM) devices and formulating appropriate design rule.[32] To elucidate the RS mechanism, current conduction behavior of the device in the LRS and HRS has been studied. I-V curves of Pt/BFO/Pt and Pt/BFCO5/Pt devices are replotted in log-log scale, as shown in Fig. 5. From the linear fitting results, both of the devices were found to exhibit the similar conduction behaviors. In LRS, the I-V relationships were found to be linear throughout the voltage range with slope ~1 indicating Ohmic

conduction. While in HRS, the conduction mechanism can be dominant uniformly by the typical trap–assisted space-charge-limited current (SCLC) conduction.[33] To clarify the type of defects/traps, XPS measurements were performed on all as grown BFO, BFCO5, BFCO10, and BFCO15 films to investigate the chemical states of different ions.

Figure 6(a) showed the XPS spectra of Fe 2p regions, where the Fe $2p_{3/2}$ and Fe $2p_{1/2}$ peak positions are at the binding energies of 710.9 and 724.6 eV, respectively. The Fe ions are identified in +3 and +2 valance states in BFO and BFCO5 films, as shown in Fig. 6(b). Whereas, in case of BFCO10 and BFCO15 films, we did not observe any signal corresponding to Fe^{2+}, and Fe 2 p peaks (Fe $2p_{3/2}$) are found to be more symmetrical and cannot be deconvoluted into two peaks as can be seen in BFO and BFCO5 films.[34] In BFCO films, Cr-ions also showed multivalent states where Cr $2p_{3/2}$ peak was found to be asymmetrical and can be deconvoluted into two peaks centred at 576.5 and 577.8 eV corresponding to Cr^{3+} and Cr^{4+} states, respectively, as shown in Figs. 6(c) and 6(d).[35] However, the Cr 2p peak intensity was found to be very less in BFCO5 film. According to defect chemistry, the presence of multivalent Fe-ions will lead to formation of oxygen vacancies which can be explained by Equation (1)
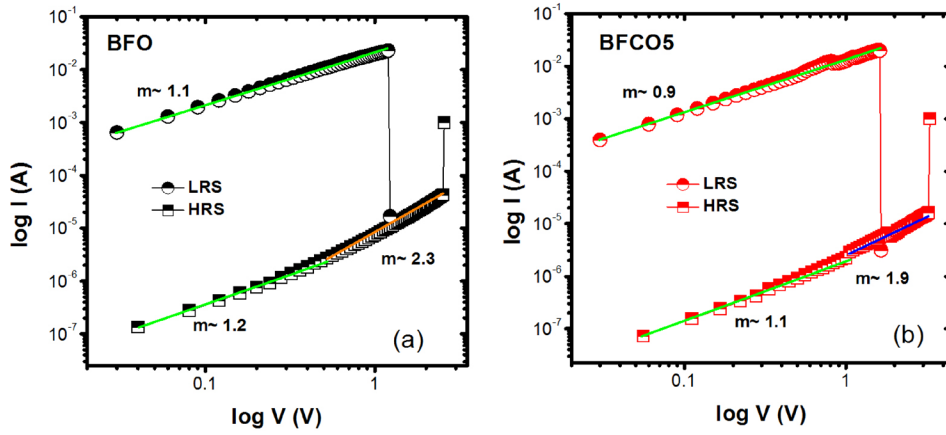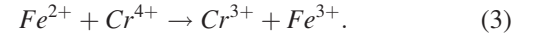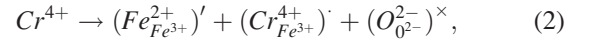
FIG. 5. log I − log V curves for LRS and HRS of (a) Pt/BFO/Pt and (b) Pt/BFCO5/Pt devices showing trap-assisted SCLC conduction mechanism in HRS and Ohmic-like conduction in LRS of the devices.

$$2\left(Fe_{Fe^{3+}}^{3+}\right)^{\times} = 2\left(Fe_{Fe^{3+}}^{2+}\right)' + \left(V_{0^{2-}}\right)^{\cdot\cdot} + \frac{1}{2}0_2. \quad (1)$$

As a consequence, the film often shows a large leakage current,[36] which can be true in case of our BFO and BFCO5 films. By increasing the doping concentration of Cr in BFO, produces more tetravalent Cr^{4+}-ions which in turn suppress the concentration of oxygen vacancies and compensate the valence fluctuation of $Fe^{2+/3+}$, as per Equations (2) and (3)

$$Cr^{4+} \rightarrow \left(Fe_{Fe^{3+}}^{2+}\right)' + \left(Cr_{Fe^{3+}}^{4+}\right)^{\cdot} + \left(O_{0^{2-}}^{2-}\right)^{\times}, \quad (2)$$

$$Fe^{2+} + Cr^{4+} \rightarrow Cr^{3+} + Fe^{3+}. \quad (3)$$

Due to the suppression of oxygen vacancies caused by high valence Cr ions, the leakage current is significantly reduced in BFCO10 and BFCO15 films, as confirmed from I-V measurements. Therefore, we suggest that the unipolar RS characteristics of BFO and BFCO5 thin films can be
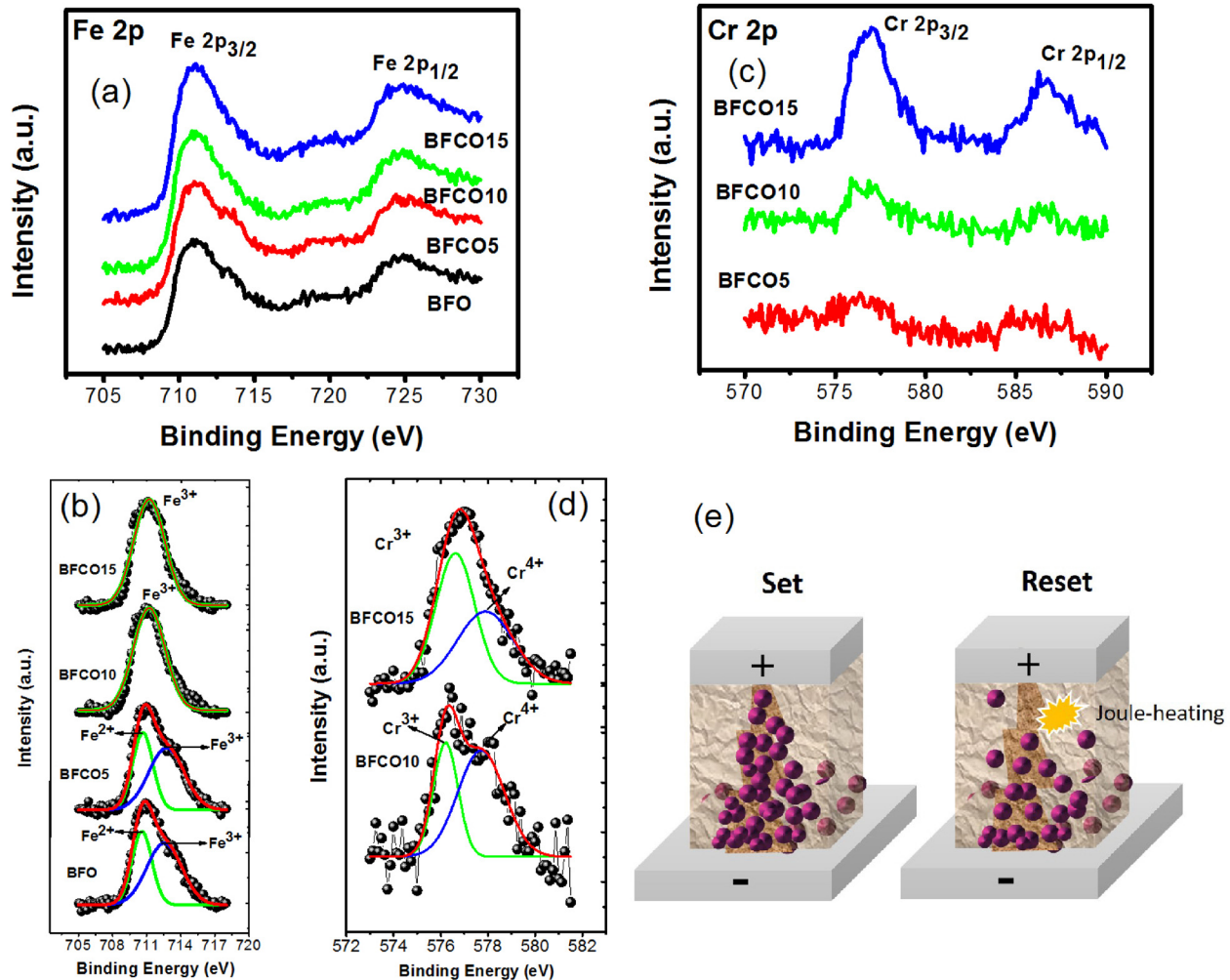

FIG. 6. (a) Fe 2p XPS spectra of the BFO, BFCO5, BFCO10, and BFCO15 thin films samples. (b) The fitting of Fe 2p$_{3/2}$ peak showing mixed valence Fe$^{2+/3+}$ states of Fe-ions in BFO and BFCO5 samples. (c) Cr 2p XPS spectra of the BFCO5, BFCO10, and BFCO15 thin films samples. (d) Cr 2p$_{3/2}$ peak is deconvoluted into two peaks corresponding to Cr^{3+} and Cr^{4+} states in BFCO10 and BFCO15 samples.

explained by electron-conducting filaments formed out of charged oxygen vacancies between cathode and anode that switch the device into ON-states, whereas thermally assisted electromigration of oxygen ions ruptures this conductive path leading to the device into OFF-state, as depicted in the schematic diagram in Fig. 6(e).[35] While, due to the less availability of oxygen vacancies, RS phenomenon was not observed in BFCO10 and BFCO15 which confirms the dominant role of oxygen vacancies towards RS behavior in BFO films.

IV. CONCLUSION

Pulsed laser deposited Cr-doped polycrystalline BFCO thin films were studied. The variation of Cr-dopant concentration was found to alter the structural, optical, magnetic, and resistive switching properties of BFO to different extents. The BFCO thin films showed higher optical band gap, improved magnetization behavior owing to super exchange interaction between aliovalent Cr and Fe-ions, and lower leakage current with increased Cr-doping concentration. Further, the BFCO films with higher Cr-concentrations were not found to show resistive switching ascribed to the high valance Cr^{4+}-ion induced annihilation of oxygen vacancies, which exhibit the crucial role of oxygen vacancies towards resistive switching phenomenon in BFO thin films.

[1] W. Eerenstein, N. D. Mathur, and J. F. Scott, Nature **442**, 759 (2006).
[2] H. Schmid, Ferroelectrics **162**, 19 (1994).
[3] N. A. Hill and A. Filippetti, J. Magn. Magn. Mater. **242**, 976 (2002).
[4] C. W. Nan, M. I. Bichurin, S. Dong, D. Viehland, and G. Srinivasan, J. Appl. Phys. **103**, 031101 (2008).
[5] G. Catalan and J. F. Scott, Adv. Mater. **21**, 2463 (2009).
[6] N. M. Murari, R. Thomas, S. P. Pavunny, J. R. Calzada, and R. S. Katiyar, Appl. Phys. Lett. **94**, 142907 (2009).
[7] C. H. Yang, J. Seidel, S. Y. Kim, P. B. Rossen, P. Yu, M. Gajek, Y. H. Chu, L. W. Martin, M. B. Holcomb, Q. He, P. Maksymovych, N. Balke, S. V. Kalinin, A. P. Baddorf, S. R. Basu, M. L. Scullin, and R. Ramesh, Nat. Mater. **8**, 485 (2009).
[8] H. T. Yi, T. Choi, S. G. Choi, Y. S. Oh, and S.-W. Cheong, Adv. Mater. **23**, 3403 (2011).
[9] S. Y. Yang, J. Seidel, S. J. Byrnes, P. Shafer, C.-H. Yang, M. D. Rossell, P. Yu, Y.-H. Chu, J. F. Scott, J. W. Ager III, L. W. Martin, and R. Ramesh, Nat. Nanotechnol. **5**, 143 (2010).
[10] R. Agarwal, Y. Sharma, and R. S. Katiyar, Appl. Phys. Lett. **107**, 162904 (2015).
[11] R. K. Katiyar, Y. Sharma, P. Misra, V. S. Puli, S. Sahoo, A. Kumar, J. F. Scott, G. Morell, B. R. Weiner, and R. S. Katiyar, Appl. Phys. Lett. **105**, 172904 (2014).
[12] R. K. Katiyar, Y. Sharma, D. Barrionuevo, S. Kooriyattil, S. P. Pavunny, J. S. Young, G. Morell, B. R. Weiner, R. S. Katiyar, and J. F. Scott, Appl. Phys. Lett. **106**, 082903 (2015).
[13] A. Anshul, H. Borkar, P. Singh, P. Pal, S. S. Kushvaha, and A. Kumar, Appl. Phys. Lett. **104**, 132910 (2014).
[14] R. L. Gao, H. W. Yang, Y. S. Chen, J. R. Sun, Y. G. Zhao, and B. G. Shen, Appl. Phys. Lett. **104**, 031906 (2014).
[15] J. A. Klug, M. V. Holt, R. N. Premnath, A. Joshi-Imre, S. Hong, R. S. Katiyar, M. J. Bedzyk, and O. Auciello, Appl. Phys. Lett. **99**, 052902 (2011).
[16] M. Park, S. Hong, J. A. Klug, M. J. Bedzyk, O. Auciello, K. No, and A. Petford-Long, Appl. Phys. Lett. **97**, 112907 (2010).
[17] Y. Sharma, P. Misra, R. K. Katiyar, and R. S. Katiyar, J. Phys. D: Appl. Phys. **47**, 425303 (2014).
[18] J. M. Luo, S. P. Lin, Yue Zheng, and B. Wang, Appl. Phys. Lett. **101**, 062902 (2012).
[19] C.-H. Yang, D. Kan, I. Takeuchi, V. Nagarajan, and J. Seidel, Phys. Chem. Chem. Phys. **14**, 15953–15962 (2012).
[20] Z. Cheng, X. Wang, S. Dou, H. Kimura, and K. Ozawa, Phys. Rev. B **77**, 092101 (2008).
[21] F. Yan, M.-O. Lai, L. Lu, and T.-J. Zhu, J. Phys. Chem. C **114**, 6994–6998 (2010).
[22] P. C. Juan, J. L. Wang, T. Y. Hsieh, C. L. Lin, C. M. Yang, and D. C. Shye, Microelectron. Eng. **138**, 86 (2015).
[23] R. Palai, H. Schmid, J. F. Scott, and R. S. Katiyar, Phys. Rev. B **81**, 064110 (2010).
[24] M. Muneeswaran and N. V. Giridharan, J. Appl. Phys. **115**, 214109 (2014).
[25] C. Himcinschi, L. Vrejoiu, T. Weibach, K. Vijayanandhini, A. Talkenberger, C. Roder, S. Bahmann, D. R. T. Zahn, A. A. Belik, D. Rafaja, and J. Kortus, J. Appl. Phys. **110**, 073501 (2011).
[26] R. Nechache, P. Gupta, C. Harnagea, and A. Pignolet, Appl. Phys. Lett. **91**, 222908 (2007).
[27] M. Murakami, S. Fujino, S.-H. Lim, C. J. Long, L. G. Salamanca-Riba, M. Wuttig, I. Takeuchi, B. Varughese, H. Sugaya, T. Hasegawa, and S. E. Lofland, Appl. Phys. Lett. **88**, 112505 (2006).
[28] W. Eerenstein, F. D. Morrison, J. Dho, M. G. Blamire, J. F. Scott, and N. D. Mathur, Science **307**, 1203 (2005).
[29] P. Baetting, C. Ederer, and N. A. Spaldin, Phys. Rev. B **72**, 214105 (2005).
[30] H. Deng, H. Deng, P. Yang, and J. Chu, J. Mater. Sci.: Mater. Electron. **23**, 1215 (2012).
[31] Y. Sharma, P. Misra, S. P. Pavunny, and R. S. Katiyar, Appl. Phys. Lett. **104**, 073501 (2014).
[32] R. Waser and M. Aono, Nat. Mater. **6**, 833 (2007).
[33] R. K. Katiyar, Y. Sharma, D. G. B. Diestra, P. Misra, S. Kooriyattil, S. P. Pavunny, G. Morell, B. R. Weiner, J. F. Scott, and R. S. Katiyar, AIP Adv. **5**, 037109 (2015).
[34] J. K. Kim, S. S. Kim, W. J. Kim, A. S. Bhalla, and R. Guo, Appl. Phys. Lett. **88**, 132901 (2006).
[35] Y. Sharma, P. Misra, and R. S. Katiyar, J. Appl. Phys. **116**, 084505 (2014).
[36] M. M. Shirolkar, C. Hao, X. Dong, T. Guo, L. Zhang, M. Li, and H. Wang, Nanoscale **6**, 4735 (2014).